Research on Water Seepage Detection Technology of Tunnel Asphalt Pavement Based on Deep Learning and Digital Image Processing

Jiaqi Li (622190970103@mails.cqjtu.edu.cn)
Chongqing Jiaotong University
Zhaoyi He
Chongqing Jiaotong University
Dongxue Li
Chongqing Jiaotong University
Aichen Zheng
Chongqing Jiaotong University

Research Article

Keywords: asphalt pavement, pavement seepage, convolutional neural network, digital image processing, water seepage geometrical characteristic

Posted Date: January 13th, 2022

DOI: https://doi.org/10.21203/rs.3.rs-1235518/v1

Abstract

In order to improve the traffic safety of the tunnel pavement and reduce the impact of water seepage on the pavement structure, a convolutional neural network (CNN) model is established based on image detection technology to realize the identification, classification and statistics of pavement seepage. First, compared with the MobileNet network model, the deep learning model EfficientNet network model was built, and the accuracy of the two models was analyzed for pavement seepage recognition. The F1 Score was introduced to evaluate the accuracy and comprehensive performance of the two models for different types of seepage characteristics. Then the three gray processing methods, six threshold segmentation methods, as well as three filtering methods were compared to extract water seepage characteristics of digital image. Finally, based on the processed image, a calculation method of water seepage area was proposed to identify the actual asphalt pavement water seepage. The result shows that the recognition accuracy of the EfficientNet network model in the training set and the validation set are 99.85% and 97.53%, respectively, and the prediction accuracy is 98.00%. The accuracy of pavement water seepage recognition and prediction is better than the MobileNet network model. Using the cvtColor function for gray processing, using THRESH_BINARY for threshold segmentation, and using a combination of median filtering and morphological opening operations for image noise reduction can effectively extract water seepage characteristics. The water seepage area calculated by the proposed method has a small difference with the actual water seepage area, and the effect is agreeable.

1. Introduction

With the increase in the number and length of highway tunnels, various tunnel diseases have gradually appeared. Water seepage is one of the main factors of tunnel diseases. Water seepage will make the road wet and slippery, causing great hidden dangers to driving safety, and serious damage to the asphalt pavement structure, which will further deteriorate the operating environment and cause traffic safety problems [1–3]. Effective water seepage detection technology plays a vital role in maintaining the asphalt pavement service status of the operating tunnel and ensuring driving safety. Traditional tunnel pavement disease detection mainly relies on manual inspection, which has disadvantages such as low efficiency, high cost, and strong subjectivity in disease evaluation [4, 5]. With the rapid development of machine learning and image processing technology, the research proposes to perceive and analyze the water seepage state of the operating tunnel pavement through digital images, which provides a basis for the assessment of the water seepage disease of the tunnel pavement.

Traditional image recognition technology mainly defines the diseased area through shallow features such as image shape, color, texture and gray value, such as histogram method, edge detection and region growing algorithm. And the image is transformed to obtain higher-level feature values for disease identification [6–8]. He et al. [9] carried out crack image testing on the pavement crack image after dimensionality reduction, gray-scale correction and filtering, determined the crack interface, and detected asphalt pavement cracks through characteristics such as inclination, Gaussian distribution and edge gradient. Chen et al. [10] independently constructed a multi-scale image analysis method to study pavement diseases. This method can effectively remove the background noise of the picture, sharpen the target edge better, and can restrain the boundary movement. Wang et al. [11] used three-dimensional laser scanning to obtain tunnel seepage disease information, enhanced the edge information of the disease through image binarization, and further analyzed the size of the disease by using a region description algorithm. These methods have a good recognition effect for simple textures, large differences in gray scale, and obvious disease characteristics. However, the effect of image recognition under complex background is not obvious.

In contrast, deep learning algorithms are completely end-to-end, without human intervention, it can automatically perform abstract expression and analysis based on the characteristics of the original image. It has excellent convenience and operability, and has attracted wide attention from the engineering community [12, 13]. Applying deep learning algorithms to the identification and classification of pavement seepage diseases can greatly reduce the feature description, extraction, and recognition based on artificial experience, which is conducive to improving the accuracy and versatility of the seepage recognition algorithm [14, 15]. Zhao et al. [16] constructed a pavement state feature database by segmenting the image, extracting 9-dimensional color feature vectors and 4 texture feature vectors, and proposed a pavement state recognition method based on Support Vector Machine (SVM) to identify wet and slippery states. Zhang et al. [17] used the SSD-mobilenet architecture to transplant to smart terminals and built a pavement disease database to identify pavement disease images. Wu et al. [18] combined DenseNet and deconvolutional network to form an end-to-end multi-scale full-convolutional neural network, which segmented and identified cracks and diseases in the complex fine-grained background of asphalt pavement.

CNN has become the most representative neural network in the field of deep learning. It can work with complex environmental information, vague background knowledge, and unclear reasoning rules [19–21]. The traditional water seepage disease recognition algorithm uses a large number of image processing processes, which takes a long time and the recognition rate and accuracy are not high [22]. However, using the CNN model does not require a large number of image processing procedures. The image can be directly used as input for training. The model can automatically learn the pixel difference of the water seepage image to quickly and accurately complete the classification target [23–25].

In this work, the model is based on the CNN and is designed in accordance with the classic network structure. The images of tunnel pavement seepage are collected, and the accuracy of the training model is tested by establishing a data set and a verification set. In order to further improve the accuracy of recognition, the extended network EfficientNnet network recognition algorithm based on the CNN backbone network is used to achieve the goal of correctly identifying road water seepage diseases. On the basis of identifying pavement seepage diseases, the geometric characteristics of pavement seepage are extracted based on semantic segmentation, and the area of seepage is calculated, which lays the foundation for maintenance evaluation.

2. Efficientnet Network

The EfficientNet network is a set of backbone feature extraction networks based on CNN proposed by Tan M et al. [26] in 2019. CNN models are usually trained under known hardware resource conditions, while EfficientNet is a model generated by the MnasNet model implemented by a reinforcement learning

algorithm. The three dimensions of the model's depth, width (the number of channels in the feature map), and resolution (the input image size) are simultaneously scaled, and finally expanded to form the EfficientNet series network models [27]. As shown in Fig. 1, the EfficientNet network model realizes the comprehensive consideration of the three factors of depth, width, and resolution. Compared with other network models, the EfficientNet series network models can maintain a high classification accuracy rate with a small number of model parameters [28, 29].

2.1 The structure of EfficientNet network model

The EfficientNet network model consists of four parts: mobile inverted bottleneck convolution (MBConv) module, convolution layer, pooling layer, and fully connected layer. MBConv is obtained through neural network architecture search, and the module structure is similar to depthwise separable convolution. It gives the model a random depth, shortens the practice required for model training, and improves the performance of the model. The function of the convolution layer is to extract different features of the input picture and hand them to the subsequent high-level neurons for processing. The first layer of convolution layer can only extract some low-level local features, such as edges, lines, and corners, and more complex features can be iteratively extracted from low-level features through more layers of convolution. Usually after the convolution layer, features with large dimensions are obtained. The role of the pooling layer is to cut the features into several regions, and remove the maximum or average value to obtain new features with smaller dimensions, while reducing the risk of overfitting. This paper use is global average pooling. The fully connected layer is to combine all the local features into a global feature, that is, to fully connect the results after convolution and pooling, and turn multi-dimensional vectors into one-dimensional vectors.

2.2 Selection of activation function

The main function of the activation function is to introduce nonlinearity into the network. If there is no activation function, the output signal will be a simple linear function with limited complexity. The mapping ability of learning complex functions from data is smaller and the ability to extract features is weakened. Commonly used activation functions include sigmoid function, Tanh function and ReLU function. The working principle of the activation function is shown in Fig. 1(a). The input layer input xi is multiplied by the weight wk and then accumulated, and the activation y is obtained through the activation function.

Compared with the underfitting problem when the input value of Tanh function is too large or too small, the ReLU function has the limitation of overfitting and forced sparse processing to cause neuron necrosis. In this paper, the Swish activation function is used. The Swish activation function is a variant of the Sigmoid activation function. The expression of the Sigmoid function is as follows:

$$Sigmoid(x) = \frac{1}{1+e^{-x}} \quad (1)$$

The expression of the Swish function is as follows, where β is an adjustable parameter:

$$Swish(x) = x \cdot Sigmoid(\beta x) \quad (2)$$

Swish function has the characteristics of no upper bound, lower bound, smooth curve, and non-monotonic function. The performance of the Swish function in shallow networks is not particularly prominent, but as the depth of the network increases, the performance of the Swish function becomes more and more prominent. The EfficientNet network selected in this paper has a more complex model and a deeper network structure, so it is more suitable to use the Swish function as the activation function.

2.3 Feature convolution module

The mobile flip bottleneck convolution first performs 1*1 point-by-point convolution on the input feature map, and changes the output channel dimension according to the expansion ratio, and then performs Batch Normalization (BN) and activation function (Swish). If the expansion ratio is 1, then directly skip the point-by-point convolution, the BN and activation functions. Then perform k*k depthwise convolution, and finally introduce compression and excitation operations, and then end with 1*1 point-by-point convolution to restore the original channel dimension.

The SENet module in the MBConv module is a feature map operation based on attention. First, the SENet module compresses the feature map, performs global average pooling in the channel dimension direction, and obtains the global feature map in the channel dimension direction. Then the global feature is excited, and the 1*1 convolution equal to the number of the global feature dimension C is multiplied by the activation ratio R to perform convolution on the feature map. Learn the relationship between each channel, and then get the weight of different channels through the Sigmoid activation function. Finally, multiply the original feature map to get the final feature.

In order to solve the gradient disappearance and gradient explosion caused by the excessive number of model convolution layers. The MBConv module introduces the short-circuit path of the residual module. It makes the gradient spread coherently in the very deep network to prevent the gradient from superimposing.

3. Design Of Water Seepage Recognition Algorithm

In order to establish a deep learning algorithm that can classify water seepage images of asphalt pavement and extract and calculate water seepage characteristics, this paper uses two models of MobileNet network and EfficientNet network to learn water seepage characteristics of asphalt pavement. The algorithm design is based on python language and keras development framework.

3.1 Data collection and processing

The model designed in this paper is mainly used to classify and identify the four types of water seepage characteristics of tunnel asphalt pavement: point seepage, line seepage, surface seepage, and no seepage, as shown in Fig. 2. Using the mobile phone, 200 pictures of each of the 4 types of water seepage characteristics of asphalt pavement in different tunnels were collected. The four types of features are labeled as A, B, C, and D respectively, and they are stored in a csv format file. Since deep learning models training require a large amount of data, and considering the time cost of collecting data in real scenes and the influence of various environmental factors, in order to ensure the diversity of data, the collected data is expanded and enhanced.

As shown in Table 1, the data set is expanded by means of flipping up and down, mirroring, changing the brightness, and Gaussian blur. The four types of pavement water seepage characteristic images were increased to 600 respectively, which basically met the requirements of model training. Not only can it effectively prevent the model from overfitting, but it can also improve the model's recognition rate of pavement seepage.

3.2 MobileNet network model construction

3.2.1 MobileNet network model

MobileNet is a typical representative of lightweight networks. It introduces deep separable convolution based on the classic CNN model, and replaces the pooling layer and part of the fully connected layer with convolution layers [30, 31]. Standard convolution is to combine a set of convolution kernels and input data into a single-channel feature output. The convolution form of depth separable convolution is factorization. The standard convolution is solved into two parts: deep convolution and point-wise convolution. A single convolution kernel of a fixed size is applied to each input channel through deep convolution, and then channel information is fused and output through point-by-point convolution.

3.2.2 Concrete model parameters

The MobileNet network model established in this paper is firstly a 3*3 standard convolution. Then pointwise convolution is used alternately with the depthwise convolution layer with a step length of 1 or 2. Then use average pooling to change the characteristic value into 1*1, and add a fully connected layer according to the prediction of four types of water seepage. Finally, there is a softmax layer. There are 28 layers of depthwise convolution and pointwise convolution in this network model.

3.3 EfficientNet network model construction

The EfficientNet network model established in this paper is divided into 9 parts, a total of 18 layers of neural networks. The first part is an ordinary convolutional layer with a convolution kernel of 3*3 and a step size of 2, which contains BN and Swish. The second part is the MBConv structures with the 3*3 convolution kernel. Part 3~8 are the MBConv structures that expand the channel of the input feature matrix to 6 times the original, and the convolution kernels are 3*3, 5*5, 3*3, 5*5, 5*5, 3*3 respectively. The 9th part consists of a 1×1 convolutional layer (including BN and Swish), an average pooling layer and a fully connected layer. The network structure is shown in Fig. 3.

As shown in Fig. 4, the MBConv structure is mainly composed of a 1*1 ordinary convolution for dimension upgrade, a deep convolution with a convolution kernel size of 3*3 or 5*5, an SE module, and a 1*1 ordinary convolution for dimensionality reduction and a dropout layer. In the SE module, the number of nodes in the first fully connected layer is 1/4 of the channels input to the MBConv feature matrix, and the Swish activation function is used. The number of nodes in the second fully connected layer is the same as the number of feature matrix channels output by the deep convolutional layer, and the Sigmoid activation function is used.

3.4 Comparison of model results

The test environment is: Windows10 operating system, Intel i7-4720HQ processor, NVIDIA GeForce RTX2060, python3.8, keras2.2.5, tensorflow1.14.0. The 2400 images after image enhancement are used as the training data set, 70% of which are used as the training set, 20% are used as the test set, and 10% are used as the validation set for testing. To ensure that the two models are performed in the same environment, the batch size is set to 32, and the number of training epochs is set to 60.

The training results of the MobileNet model and the EfficientNet model are shown in Fig. 5.

As shown in Fig. 5, the accuracy of the first epoch training set is 83.84%, and the loss value is 0.3929. After 60 epochs of training, the accuracy of the model in the training set is 97%, and the loss value is 3.4×10-4. The accuracy rate of the validation set increased from 70.07–96.77%, an increase of 26.7%, and the loss value was reduced from 0.8786 to 0.0527, a decrease of 0.8259. In the whole training process, the accuracy rate increases with the increase of the training, and the loss decreases with the increase of the training, which meets the training requirements as a whole. However, the fluctuations in the accuracy and loss of the verification set are significantly larger than that of the training set. This is due to the fact that the amount of data in the verification set is less than that of the training set, and does not affect the judgment of the result.

After 60 epochs of training, the accuracy of the EfficientNet model training set has been increased from 90.88–99.85%, and the loss has been reduced from 0.2318 to 1.67×10-5. The accuracy of the validation set has increased from 93.83–97.53%, an increase of 3.7%, and the loss has been reduced from 0.2976 to 0.1023, which is a decrease of 0.1973. Compared with the MobileNet model, the EfficientNet model validation set has a smaller range of accuracy and loss, and the model has a better recognition effect for images.

In order to further compare the accuracy of the two models for the prediction of water seepage feature images, the F1 Score index is introduced for evaluation. F1 Score takes into account the precision and recall of the classification model, and is the harmonic average of the accuracy and recall of the model. The equation is as follows:

$$Pr = \frac{TP}{TP+FP} \quad (3)$$

In the Eq. (3): Pr is the accuracy rate; TP is the true positive prediction; FP is the false positive prediction.

$$Re = \frac{TP}{TP+FN} \quad (4)$$

In the Eq. (4): Re is the recall rate; FN is the false negative prediction.

$$F1\,Score = \frac{2 \cdot Pr \cdot Re}{Pr+Re} \quad (5)$$

Randomly select 200 images in the data set for prediction. Among them, there are 34 point seepage images, 42 line seepage images, 64 surface seepage images, and 60 no seepage images. Evaluate the results of each type of prediction and use the weighted average to obtain the average F1 Score of the model. The results are shown in Table 2.

It can be seen from the table that the prediction accuracy of the MobileNet network model for point seepage is 95.5%, the prediction accuracy for line seepage is 94.0%, the prediction accuracy for surface seepage is 91.5%, and the prediction accuracy for no seepage is 99.0%. After training, the MobileNet network model has an average prediction accuracy of 95.0% for the four types of water seepage characteristics. The EfficientNet network model has a prediction accuracy of 98.0% for point seepage, 97.5% for line seepage, 97.0% for surface seepage, and 99.5% for no seepage. In the prediction of the four types of water seepage characteristics, the prediction accuracy of the EfficientNet network model is higher than that of the MobileNet network model, and the average prediction accuracy of the EfficientNet network model is 98.0%, which is 3% higher than that of the MobileNet network model.

The average F1 Score of the two models reached more than 90%, and both models can identify pavement water seepage characteristics very well. The EfficientNet network model predicts four types of water seepage characteristics not only in accuracy, but also in precision, recall and F1 Score higher than MobileNet. And the average F1 Score is 5.98% higher than MobileNet. It shows that the EfficientNet network model is more accurate for pavement water seepage recognition and has better performance.

4. Geometric Characteristics Of Pavement Water Seepage

After the pavement water seepage images are classified, further information such as the shape and area of the road water seepage need to be obtained before the driving safety and the degree of pavement damage can be evaluated. The collected pavement water seepage set contains most of the pavement information, and image processing technologies need to be used to effectively extract the image water seepage information to reduce the interference caused by other information and provide data for road condition evaluation.

4.1 Image processing

In order to ensure that high quality water seepage characteristic information can be obtained, reduce the loss of water seepage information caused during image processing, and improve the accuracy of water seepage geometric feature extraction, the resolution of the picture is uniformly adjusted to 3500×3500 before image processing.

4.1.1 Gray processing

Since the collected pavement water seepage images are all color digital images, the color of each pixel depends on the color components R, G, and B, each component has 255 values that can be taken, and the color range of a pixel point is 255*255*255. After the color images are gray scaled, the R, G, and B components of each pixel are the same, and each pixel has only 255 color ranges, which greatly reduces the amount of image calculation and recognition time. Like color images, grayscale images also reflect the overall image, the distribution and characteristics of the layout chromaticity and grayscale levels.

This paper uses three gray processing methods, namely: cvtColor, meanGray and maxGray.

It can be seen from Fig. 6 that after using the maxGray, the overall image is dark. Although it is beneficial to more complete extraction of water seepage characteristics, it will cause a lot of unnecessary noises when thresholding the image, which increases the difficulty of image processing. After the meanGray, the edge pixels of the water seepage characteristics are similar, and the edge contour of the water seepage characteristics cannot be well recognized. After using the cvtColor, the edges contour of the water seepage characteristics are obvious, and the feature pixels of high and low brightness are better improved. Compared with the other two methods, the water seepage characteristics are more obvious. Therefore, cvtColor is selected as the method for gray processing.

4.1.2 Threshold segmentation

Threshold segmentation is binarization. The target feature is separated from the image background according to a certain threshold, and the image can be segmented by using the gray difference between the target feature area and the background area. The image after binarization has only two colors of black and white, that is, the gray value is only 0 and 255, which can better highlight the characteristic area of water seepage.

The six threshold segmentation methods used in this article are: Between-cluster variance method (OTSU), THRESH_BINARY, THRESH_BINARY_INV, THRESH_TRUNC, THRESH_TOZERO, THRESH_TOZERO_INV.

According to many tests, when the threshold is set to 65, the water seepage characteristics are displayed intact, and the image is in the best state. The image processed by the above method is shown in Fig. 7.

It can be seen from Fig. 7 that since the asphalt pavement and water seepage characteristics are all black in different degrees under natural conditions, after the gray processing, similar gray levels will be obtained. Therefore, when the OTSU is used, the foreground and the background cannot be distinguished more accurately. A certain gray level is also retained in THRESH_TRUNC. Although the water seepage characteristic area is more prominent than the gray processing, the background is not completely eliminated, which is not conducive to the subsequent extraction of geometric features. Although THRESH_BINARY will produce some small connected domain noise, it shows relatively obvious water seepage characteristics compared with THRESH_TOZERO and THRESH_TOZERO_INV. Therefore, the THRESH_BINARY method is selected as the threshold segmentation method of water seepage images.

4.1.3 Image denoising

Image noise is a random change of image color, which is unavoidable during image shooting and transmission, and is redundant interference information. In the asphalt pavement, because the asphalt, aggregate and water seepage colors are similar, a lot of noise will be generated. These noises do not belong to the scope of water seepage, but they will be included in the scope of water seepage area when calculating the geometric characteristics of water seepage. In order to eliminate this effect, the image needs to be denoised. After a large number of experiments, it is found that the effect of using a single method to reduce noise is not very obvious. This paper uses Gaussian filtering combined with morphological open operation and median filter combined with morphological open operation to reduce noise.

It can be seen from Fig. 8 that the noise reduction effect of the noise reduction method combining Gaussian filtering with a kernel of 5*5 and morphological open operation is not very obvious, and the image still has a lot of noise, which cannot highlight the water seepage characteristics. Compared with the former, the method of median filter combined with morphological open operation can reduce most of the noise in the images, has a better filtering effect on salt and pepper noise, and has less loss of water seepage characteristics. Therefore, the method of median filter combined with morphological open operation is used to reduce the noise of the image.

4.1.4 Removal of small connected domains

After the image noise is reduced, there are still many small black pixels that are not characteristic of water seepage. These small connected domains composed of adjacent pixels with the same pixel level have a great impact on the accumulation of subsequent water seepage characteristic pixels. The definition of connected domains is generally divided into two types, one is 4 domains and the other is 8 domains. In order to reduce the loss of edge pixels of the water seepage feature on the basis of removing the connected domains of the no seepage characteristic. The black connected domain around the seepage feature is removed by the 4 domains method. For the pixels in the water seepage characteristic that were lost in the previous image processing, an 8 domains method is used to fill in. This makes the water seepage characteristic pixels more complete and closer to the actual water seepage area. The water seepage characteristics removed by the small connected domains are shown in Fig. 9.

4.2 Extraction of pavement water seepage geometric features

The processed images only have water seepage characteristics. In the image, pixels with a level of 0 are all water seepage characteristics. Through statistics and analysis of pixels with a level of 0, a method for extracting geometric information of pavement water seepage is proposed. Establish a coordinate system (x, y, z) based on the space where the actual pavement is located, and the pavement level coincides with the xoz plane of the coordinate system. The imaging plane coordinate system (u, v) is established for the plane where the camera is located, and the uv plane is parallel to the xoz plane. Through the measurement of the actual pavement, the length and width information of the xoz plane collected in the image is obtained, and a proportional relationship is established between the length and width pixels of the uv plane. Through scale conversion, the actual pavement length represented by each pixel and the actual road pavement information represented by one pixel can be accurately obtained. Through the accumulation of pixels, the actual pavement water seepage area and other information can be obtained.

As shown in Fig. 10, in order to avoid the interference of the shooting angle and shooting distance on the the accuracy of water seepage feature recognition, it is necessary to fix the camera parameters and the height and angle of the device. In this experiment, the height of the camera from the ground is fixed at 150cm, the optical axis of the camera is perpendicular to the pavement level, the aspect ratio of the photo is 1:1, and the image pixels are 3500×3500.

From Table 3, the average error of point seepage is 7.40%, the average error of line seepage is 8.05%, and the average error of surface seepage is 9.33%. The effects of this method in the extraction of point seepage areas and line seepage areas are better than that of surface seepage areas. It may be that the water seepages at the edges of the surface seepage are filtered when the images are filtered, which makes the error between the predicted water seepage area and the actual water seepage area larger. The average error of the three types of water seepage area extraction is 8.30%, which is controlled within 10%. It shows that this method has a good effect on the extraction of water seepage geometric features.

5. Conclusion

(1) Compared with the MobileNet network model, the accuracy of the EfficientNet network model for pavement water seepage recognition is 96.01%, which is 5.98% higher than the 90.03% of the MobileNet network model. It shows that the EfficientNet network model can better identify pavement water seepage.

(2) By comparison, cvtColor can be used for gray processing, the THRESH_BINARY method can be used to threshold the image, and the combined median filter and morphological open operation can be used to reduce image noise. Using these methods for image processing can make the water seepage characteristics of the image more prominent.

(3) By using the calculation method of water seepage area, the geometric characteristics and areas of pavement water seepage can be obtained more accurately. Compared with the actual pavement water seepage information, the error is within 10%, and the effect is satisfactory.

Declarations

All authors certify that they have no affiliations with or involvement in any organization or entity with any financial interest or non-financial interest in the subject matter or materials discussed in this manuscript.

Funding

This research was funded by the National Key R&D Program of China, grant number 2018YFB1600200 and Graduate Scientific Research and Innovation Foundation of Chongqing, China, grant number CYB20177.

Author Contributions

J.L. and Z.H. conceived and designed the experiments; J.L. and A.Z. conducted the experiments; J.L. analyzed the data; J.L., Z.H., D.L., and A.Z. wrote and edited the article.

References

1. Gong XN, Guo PP. Prevention and mitigation methods for water leakage in tunnels and underground structures. *China Journal of Highway and Transport* **34**(**07**), 1–30, DOI: 10.19721/j.cnki.1001-7372.2021.07.001 (2021).
2. Shi JX, Zhang Z, Zhang XK, Ma T, Zhang HM. Research on influencing factors of tunnel water leakage diseases. *Chinese Journal of Underground Space and Engineering* **17**(**04**), 1291-1297+1321, DOI: 1673-0836(2021)04-1291-07 (2021).
3. Gao JS. Study on highway tunnel water leakage mechanisms and countermeasures. MSc Thesis, Central South University, Changsha, China (2014).
4. Wang FR. Research on infrared feature recognition and extraction of tunnel leakage. MSc Thesis Huazhong University of Science and Technology, Wuhan, China (2018).
5. Huang YJ, Liu X, Yuan Y, Liu CM, Wang XZ. Auto inspection technology for detecting leakage in a shield tunnel. *Journal of Shanghai Jiaotong University* **46**(**01**), 73-78, DOI: 10.16183/j.cnki.jsjtu.2012.01.016 (2012).
6. Gao JZ, Ren MW, Yang JY. A practical and fast method for non-uniform illumination correction. *Journal of Image and Graphics* (**06**), 30–34 (2002). https://kns.cnki.net/kcms/detail/detail.aspx?dbcode=CJFD&dbname=CJFD2002&filename=ZGTB200206004&uniplatform=NZKPT&v=RLOrictP75Gv-ul_s34Fz4R_XA-Jmv5p5mPy9c9gNhSBHu1VWnFVIiHUlFOj9I4f
7. Faisal R, Ahlan M, Mutiawati C, Rozi M, Zulherriet. The comparison between the method of Bina Marga and the pavement condition index (PCI) in road damage condition evaluation (case study: Prof. Ali Hasyimi Street, Banda Aceh). *IOP Conference Series: Materials Science and Engineering* **1087**(**1**), 012028-. DOI: 10.1088/1757-899X/1087/1/012028 (2021).
8. Duan Y, Li CS, Yan Y. Terrain classification method based on the support vector machine. *Journal of Hebei Agricultural University*, **39**(**06**), 124–129, DOI: 10.13320/j.cnki.jauh.2016.0145 (2016).
9. He LL, ZHU H, Gao ZX. A novel asphalt pavement crack detection algorithm based on multi-feature test of cross-section image. *Traitement du signal*, **35**(**3-4**), 289-302, DOI: 10.3166/TS.35.289-302 (2018).
10. Chen LL. Research and analysis of pavement disease detection method based on multi-scale image analysis. MSc Thesis, Nanjing University of Science and Technology, Nanjing, China (2009).
11. Wang Y, Liu J, Kong XS, Zhao M. Rapid detection of subway tunnel leakage based on image segmentation. *Bulletin of Surveying and Mapping*, (**08**), 78-82, DOI: 10.13474/j.cnki.11-2246.2021.0245 (2021).
12. Cheng GL. *et al*. Recognizing road from satellite images by structured neural network. *Neurocomputing*, **356**, 131–141, DOI: 10.1016/j.neucom.2019.05.007 (2019).
13. Nolte M, Kister N, Maurer M. Assessment of deep convolutional neural networks for road surface classification. 21st International Conference on Intelligent Transportation Systems (ITSC), November 04-07, Maui, HI, USA (2018).
14. Ren YP. *et al*. Image-based concrete crack detection in tunnels using deep fully convolutional networks. *Construction and Building Materials*, **234**(**C**), 117367-117367, DOI: 10.1016/j.conbuildmat.2019.117367 (2020).
15. Ye XW, Jin T, Chen PY. Structural crack detection using deep learning–based fully convolutional networks. *Advances in Structural Engineering*, **22**(**16**), 3412–3419, DOI: 10.1177/1369433219836292 (2019).
16. Zhao JD, Wu HQ, Chen LL. Road Surface State Recognition Based on SVM Optimization and Image Segmentation Processing. *Journal of Advanced Transportation*, 1–21, DOI: 10.1155/2017/6458495 (2017).
17. Zhang K, Li HW, Wang ZW, Zhao XF. Feature recognition and detection for road damage based on intelligent inspection terminal. Conference on Smart Structures and NDE for Industry 4.0, Smart Cities, and Energy Systems, April 27-May 08, ELECTR NETWORK (2020).
18. Wu YX, Yang WT, Pan JX, Chen P. Asphalt pavement crack detection based on multi-scale full convolutional network. *Journal of Intelligent & Fuzzy Systems*, **40**(**1**), 1495–1508, DOI: 10.3233/JIFS-191105 (2021).
19. Sha AM, Tong Z, Gao J. Recognition and measurement of pavement disasters based on convolutional neural networks. *China Journal of Highway and Transport*, **31**(**01**), 1–10, DOI: 10.19721/j.cnki.1001-7372.2018.01.001 (2018).

20. Xue YD, Gao J, Li YC, Huang HW. Optimization of shield tunnel lining defect detection model based on deep learning. *Journal of Hunan University (Natural Science Edition)*, **47**(**07**), 137-146, DOI: 10.16339/j.cnki.hdxbzkb.2020.07.016 (2020).
21. Cao ZJ, Lee HJ. Learning Multi-Scale Features and Batch-Normalized Global Features for Person Re-Identification. *IEEE ACCESS*, 8: 184644–184655, DOI: 10.1109/ACCESS.2020.3029594 (2020).
22. Liu XZ, Sang YL, Su YF. Detection technology of tunnel leakage disaster based on digital image processing [J]. Chinese Journal of Rock Mechanics and Engineering, **31**(**S2**), 3779–3786 (2012). https://kns.cnki.net/KXReader/Detail?invoice=xJeah%2BlKrjdXSc%2B5MmBSS3e4PzyboMoHn2aMtq2bhGu9uZWgQNi%2FW6a9IM%2F1db2GLG%2Ba5nT8CmbPSKol7TZeF16jClmjY3TJEZ8h
23. Zhang WG. *et al.* Research on pavement crack detection technology based on convolution neural network. *Journal of Central South University (Natural Science Edition)*, **52**(**07**), 2402–2415, DOI: 10.11817/j.issn.1672-7207.2021.07.026 (2021).
24. Chen LY. *et al.* Review of Image Classification Algorithms Based on Convolutional Neural Networks. *Remote Sensing*, **13**(**22**), 4712-4712, DOI: 10.3390/RS13224712 (2021).
25. Han X, Han L, Li LZ, Li HH. High-resolution remote sensing image building change detection based on deep learning. *Progress in Laser and Optoelectronics*: 1–14 [2021-11-15] (2021). http://kns.cnki.net/kcms/detail/31.1690.TN.20210823.1125.002.html.
26. Tan MX, Le Q. EfficientNet: Rethinking Model Scaling for Convolutional Neural Networks. *CoRR*, abs/1905.11946 (2019).
27. Wang C, Tang Y, Zhang XF, Liu C, Li DL. An intelligent magnetic particle testing method for forgings based on the improved EfficientNet. *Chinese Journal of Scientific Instrument*: 1-9 [2021-11-15]. http://kns.cnki.net/kcms/detail/11.2179.th.20210826.1356.002.html (2021).
28. Qiu TH, Chen SR. EfficientNet based dual-branch multi-scale integrated learning for pedestrian re-identification. *Computer application*: 1-8 [2021-11-15] (2021). https://kns.cnki.net/kcms/detail/detail.aspx?dbcode=CAPJ&dbname=CAPJLAST&filename=JSJY2021092900A&uniplatform=NZKPT&v=5lc3RO-EUUDaWS1GGODgHt0_G8DcarTHWoNLUX-EGw1L8mN95e7esttjn342fHUH
29. Linh T. D, Phuong T.N, Claudio DS, Davide DR. Automated fruit recognition using EfficientNet and MixNet. *Computers and Electronics in Agriculture*, **171**(**C**), 105326-105326, DOI: 10.1016/j.compag.2020.105326 (2020).
30. Widiansyah M, Rasyid S, Wisnu P, Wibowo A. Image segmentation of skin cancer using MobileNet as an encoder and linknet as a decoder. *Journal of Physics: Conference Series*, **1943**(**1**), DOI: 10.1088/1742-6596/1943/1/012113 (2021).
31. Chen ZC, Jiao HN, Yang J, Zeng HF. Garbage image classification algorithm based on improved MobileNet v2. *Journal of Zhejiang University (Engineering Science Edition)*, **55**(**08**), 1490–1499, DOI: 10.3785/j.issn.1008-973X.2021.08.010 (2021).

Tables

Due to technical limitations, table 1 & 3 is only available as a download in the Supplemental Files section.

Table 2
Statistics table of water seepage prediction results

Model	Characteristic type	TP	FP	FN	TN	Pr	Re	F1 Score	Average F1 Score
Mobilenet	point seepage	28	3	6	163	0.9032	0.8235	0.8615	0.9003
	line seepage	35	5	7	154	0.8750	0.8333	0.8537	
	surface seepage	59	11	5	125	0.8310	0.9219	0.8741	
	no seepage	58	0	2	140	1	0.9667	0.9831	
EfficientNet	point seepage	32	2	2	164	0.9411	0.9412	0.9412	0.9601
	line seepage	39	1	3	156	0.9750	0.9286	0.9398	
	surface seepage	62	4	2	132	0.9394	0.9688	0.9538	
	no seepage	59	0	1	148	1	0.9833	0.9916	

Figures

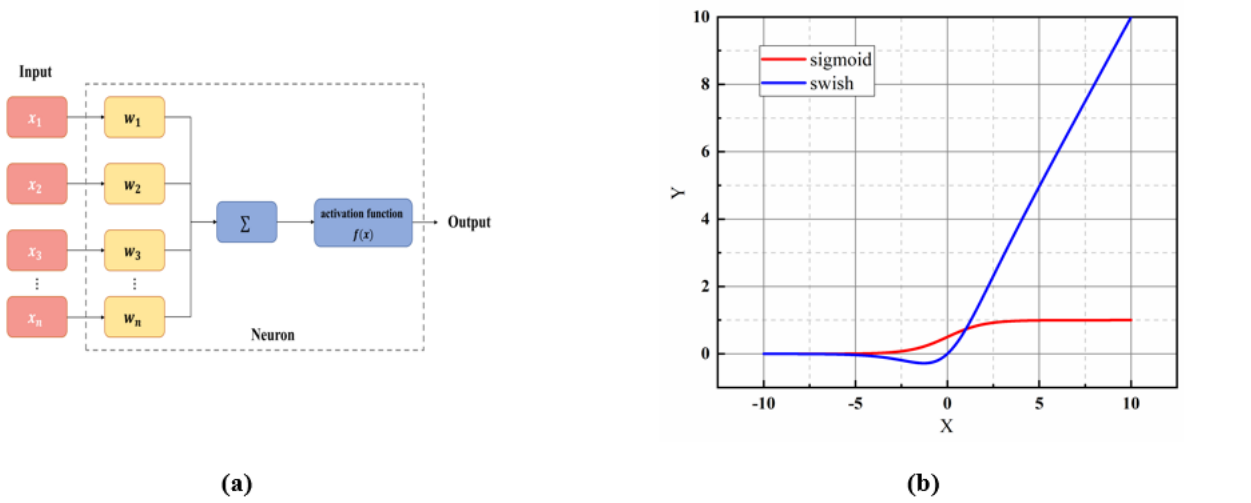

Figure 1

Activation function (a) Activation function flowchart; (b) Sigmoid activation function and Swish activation function

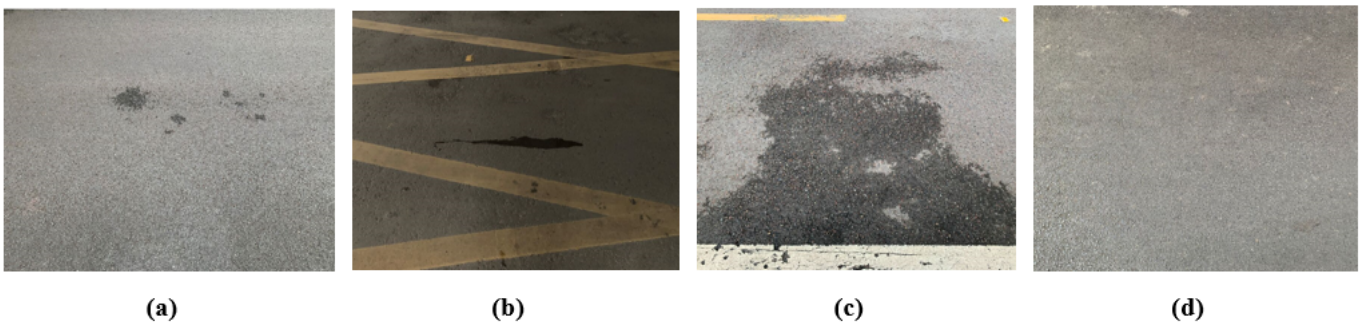

Figure 2

Classification of different water seepage characteristics (a) point seepage; (b) line seepage; (c)surface seepage; (d) no seepage

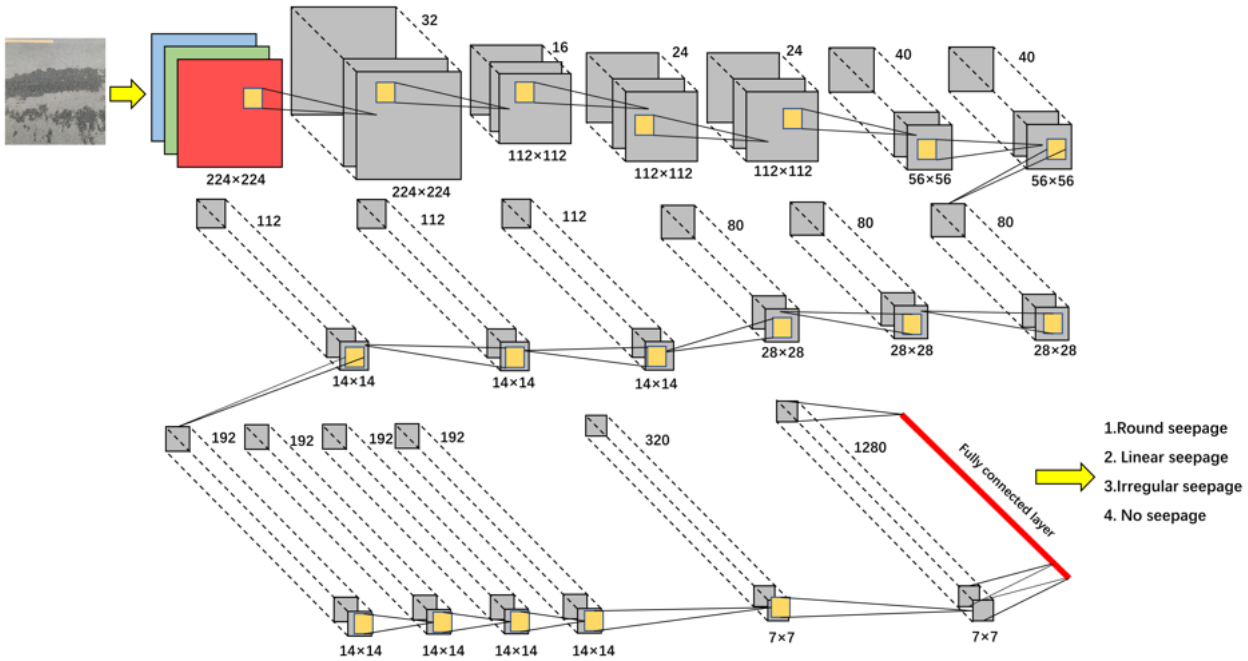

Figure 3

EfficientNet network structure

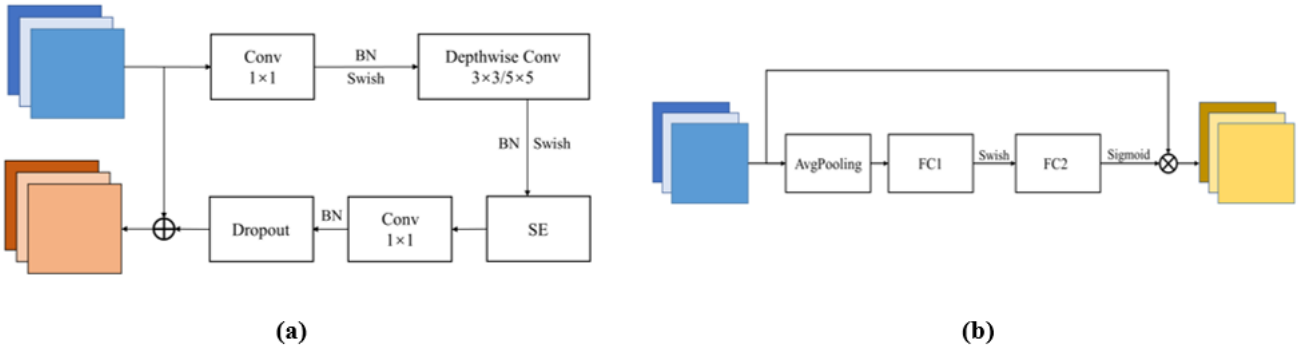

Figure 4

MBConv module and SE module (a) MBConv module; (b) SE module

Figure 5

The MobileNet model and the EfficientNet model training results (a) Line graph of the accuracy of the training set and validation set with the epoch of training; (b) Line graph of the loss value of the training set and the validation set with the epoch of training

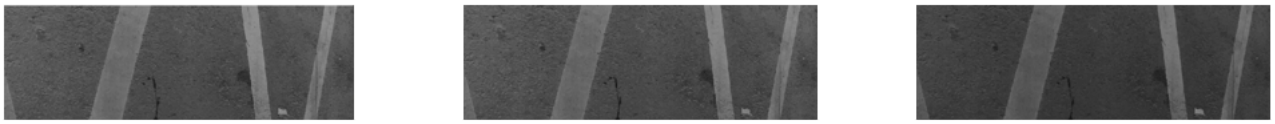

Figure 6

Image gray processing (a) cvtColor; (b) meanGray; (c) maxGray

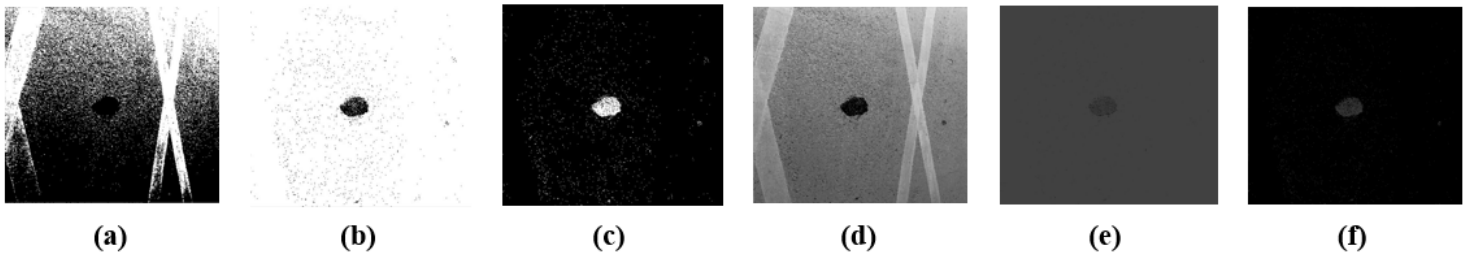

Figure 7

Threshold segmentation (a) OTSU; (b) THRESH_BINARY; (c) THRESH_BINARY_INV; (d) THRESH_TRUNC; (e) THRESH_TOZERO; (f) THRESH_TOZERO_INV

Figure 8

Image denoising (a) Gaussian filtering combined with morphological open operation: 1) point seepage; 2) surface seepage; 3 surface seepage; 4) line seepage; (b) median filter combined with morphological open operation: 1) point seepage; 2) surface seepage; 3 surface seepage; 4) line seepage

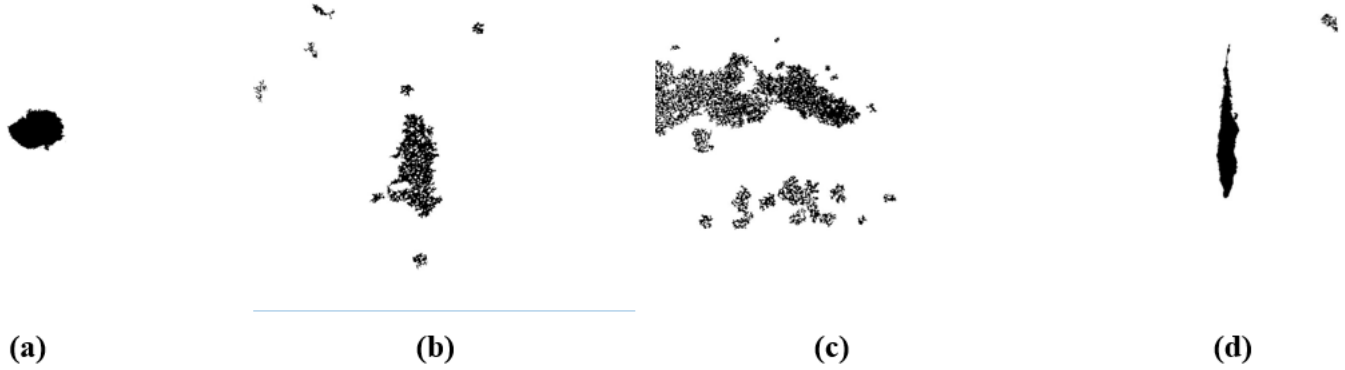

Figure 9

Water seepage feature images after removing small connected domains (a) point seepage; (b) surface seepage; (c) surface seepage; (d) line seepage

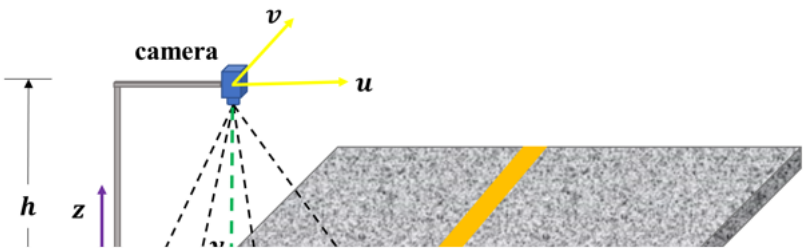

Figure 10

Field collection device

Supplementary Files

This is a list of supplementary files associated with this preprint. Click to download.

- Table13.docx